Stochastic Resonance-Based Power Amplifier Design for Orthogonal Frequency-Division Multiplexing Signals

Masanori Hamamura, *Member, IEEE,* and Izzat Darwazeh, *Senior Member, IEEE*

***Abstract*—A stochastic resonance-based power amplifier (PA) is proposed for linearly and efficiently amplifying signals with large envelope fluctuations such as those transmitted in orthogonal frequency-division multiplexing (OFDM) systems. The proposed architecture uses a Collins summing network in conjunction with a bandpass filter. The performance of the proposed PA is evaluated through the amplification of OFDM signals in terms of bit-error rate characteristics for both uncoded and coded message symbols. It is demonstrated that the performance improves as the number of parallel paths in the summing network increases, with a significant performance gain being obtained even for a moderate number of parallel paths.**

***Index Terms*—Stochastic resonance, power amplifier, delta-sigma modulation, constant envelope, switch-mode power amplifier, OFDM.**

I. Introduction

STOCHASTIC resonance (SR) is a phenomenon in which perturbations or fluctuations in a nonlinear system enhance the response to a weak input signal. SR was introduced by Benzi *et al.* [1] to explain global climate changes that occur in a 10^5-year cycle [2]. Nowadays, nonlinear effects that improve the output of a system by adding appropriate noises are widely referred to as the SR effect. Recently, Nakashima *et al.* have shown that four-level pulse-amplitude modulation (PAM) signals are detectable using a one-bit comparator output with the aid of noise [3]. Tatematsu *et al.* discussed the use of a few-bit analog-to-digital converter (ADC) for an SR-based receiver [4]. Collins *et al.* discussed waveform reconstruction using a summing network with N excitable units of a FitzHugh–Nagumo model neuron [5], and it was also applied to the ADCs [6]–[8]. A floating-gate-based neurons were discussed for the summing network [9]. In this paper, we show that Collins summing network, using simplified excitable units of signum functions, is applicable to power amplifier (PA) designs suitable for the transmission of signals with high peak-to-average power ratio (PAPR). Orthogonal frequency-division multiplexing (OFDM) signals are a typical example of high PAPR signals and require linear PA for low-distortion transmission. However, it is known that the basic linear PAs significantly degrade the transmission power efficiency. For example, when the PAPR is 10 dB, the average drain efficiency is 5% for an ideal class-A amplifier and 28% for an ideal class-B amplifier [10]. When more realistic input-output characteristics of PAs are taken into account, the efficiency becomes even significantly lower [11]. Therefore, there is a long history of improvements in PA design [12]. The Doherty [13], [14] and Chireix outphasing [15]–[17] architectures are popular, and the Kahn envelope elimination and restoration (EER) architecture and envelope tracking technique are also being studied [18], [19]. However, to the best of our knowledge, PA design using the SR effect has not yet been reported.

This paper is organized as follows. Collins summing network is introduced, and the basic concept of the PA design is described in Section II. In Section III, the SR-based PA (SRPA) design for OFDM signals is elaborated, and the bit-error rate (BER) performance of OFDM signals amplified by SRPAs is shown in Section IV. The conclusion is given in Section V.

Notations: Continuous-time signals are expressed with t in parentheses, as in $f(t)$, and their discrete-time versions are expressed with the subscript i, as in f_i. Vector forms of signals are denoted by boldface letters, as in $\mathbf{f}$, whose ith entry is f_i. The notations $(\cdot)^{\mathcal{T}}$ and $(\cdot)^{\mathcal{H}}$ stand for transpose and Hermitian transpose operations, respectively. $\delta_{i,j}$ is the Kronecker delta defined as $\delta_{i,j} = \{1(i = j), 0(i \neq j)\}$, and $\mathrm{E}[\cdot]$ is the expectation operator. $\Re[\cdot]$ and $\Im[\cdot]$ are the real and imaginary parts of a complex number, respectively. $|\cdot|$ is the modulus of a complex number and $\mathrm{j} = \sqrt{-1}$. The symbol $*$ denotes the convolution operation and $f_i \leftrightarrow F_k$ denotes that f_i and F_k are the discrete Fourier transform (DFT) pair.

II. Summing network and waveform reconstruction

We begin by considering waveform reconstruction using a summing network of N excitable units with the aid of noises [5], as shown in Fig. 1. In this study, the signum function $\mathrm{sgn}(x) = \{+1\ (x > 0), -1\ (x < 0)\}$ $(x \in \mathbb{R})$ is used for excitable units as shown in Fig. 1. Signals $s_n(t)$ $(n = 1, 2, ..., N)$ are the sums of a common source signal

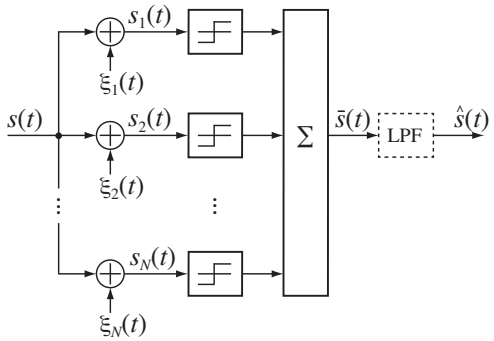

Fig. 1. Summing network of N excitable units of signum functions for waveform reconstruction with the aid of noises.

Manuscript received April XX, 2024; revised August XX, 2024.

M. Hamamura is with the School of Informatics, Kochi University of Technology, Kochi 782-8502, Japan (e-mail: hamamura.masanori@kochi-tech.ac.jp).

I. Darwazeh is with the Department of Electronic and Electrical Engineering, University College London, WC1E 7JE London, U.K. (e-mail: i.darwazeh@ucl.ac.uk).

$s(t)$ and independent noises $\xi_n(t)$, and are summed together through the signum functions $\mathrm{sgn}(x)$ to produce a reconstructed signal $\bar{s}(t)$. We assume that the source signal $s(t)$ is a band-limited zero-mean Gaussian random process with a unit variance of $\mathrm{E}[s^2(t)] = 1$ and the noises $\xi_n(t)$ are zero-mean Gaussian random processes with an identical variance of $\mathrm{E}[\xi_n^2(t)] = \sigma^2$. Therefore, the signal-to-noise ratio SNR of $s(t)$ and $\xi_n(t)$ is represented as $\mathrm{SNR} = \mathrm{E}[s^2(t)]/\mathrm{E}[\xi_n^2(t)] = 1/\sigma^2$ for all n.

Let s_i $(i = 1, 2, ..., M_s)$ be a discrete-time representation of the source signal $s(t)$ sampled at time $t = (i-1)\Delta_t$, where $\Delta_t = T_N/R_{\mathrm{os}}$ is the sampling time interval, $T_N = (2B)^{-1}$ is the Nyquist interval, B is the bandwidth of $s(t)$, and R_{os} is the oversampling ratio. Again, let $\xi_{n,i}$ be the discrete-time signals of the noises $\xi_n(t)$ sampled at time $t = (i-1)\Delta_t$. We assume that $\mathrm{E}[\xi_{n,i}\xi_{m,j}] = \delta_{n,m}\delta_{i,j}\sigma^2$.

Next, to assess the accuracy of reconstruction, we study the cross-correlation between the source and reconstructed signals.

A. Average Cross-Correlation Between Source and Reconstructed Signals

Let $\mathbf{s} \in \mathbb{R}^{M_s \times 1}$ be a source signal vector and $\bar{\mathbf{s}} \in \mathbb{R}^{M_s \times 1}$ be a reconstructed signal vector whose ith entry is $\bar{s}_i = \sum_{n=1}^{N} \mathrm{sgn}(s_i + \xi_{n,i})$. Using $\mathbf{s}$ and $\bar{\mathbf{s}}$, we obtain the cross-correlation value between the source signal $s(t)$ and the reconstructed signal $\bar{s}(t)$ such that $\mathbf{s}^{\mathcal{T}}\bar{\mathbf{s}}/(\sqrt{\mathbf{s}^{\mathcal{T}}\mathbf{s}}\sqrt{\bar{\mathbf{s}}^{\mathcal{T}}\bar{\mathbf{s}}})$.

Figure 2(a) shows the cross-correlation values, averaged over 500 Monte Carlo simulation trials, as a function of SNR, for N = 1, 10, 100, and 1000, where $R_{\mathrm{os}} = 8$ and the observation period for each trial was chosen to be $0 \le t < 100T_N$ (i.e., $M_s = 800$).[1]

It is observed from Fig. 2(a) that the average cross-correlation value for N = 100 or 1000 reaches more than 0.95 if SNR is appropriately chosen. In other words, appropriate values of the noise variance σ^2 improve the quality of waveform reconstruction. It should be noted that for all values of N, the cross-correlation values converge to a specific value of 0.8 as the SNR becomes large. This is due to the fact that all N outputs $\mathrm{sgn}[s_n(t)]$ from the signum functions in Fig. 1 become an identical waveform $\mathrm{sgn}[s(t)]$ if SNR $\to \infty$. Consequently, the summed signal $\bar{s}(t)$ of these waveforms becomes $\bar{s}(t) = N \cdot \mathrm{sgn}[s(t)]$, which is still binary in $\{+N, -N\}$. Thus, N is irrelevant for the cross-correlation value if SNR $\to \infty$.

This waveform reconstruction can be expressed as follows: For a certain normalization constant $\beta \in \mathbb{R}$, $\beta\bar{s}(t)$ asymptotically approaches $s(t)$ for $N' \to \infty$ with respect to (wrt) the cross-correlation criterion if SNR is appropriate, where

$$\bar{s}(t) = \sum_{n=1}^{N'} \mathrm{sgn}[s(t) + \xi_n(t)]. \tag{1}$$

The symbol N' was used instead of N in (1) for some reason as will be apparent shortly.

[1]The source signal $s(t)$ was produced with a sum of L sinusoidal waves $\sqrt{\frac{2}{L}}\cos(2\pi f_l t + \theta_l)$ $(l = 1, 2, ..., L)$, where θ_l are independent random numbers with a uniform distribution in $(0, 2\pi)$. To prevent $s(t)$ from being periodic, the frequencies f_l are also randomly chosen with uniform distributions in unoverlapped frequency bins $((l-1)\frac{B}{L}, l\frac{B}{L})$. For each trial, independent random numbers are generated and altered. $L = 30$ was chosen.

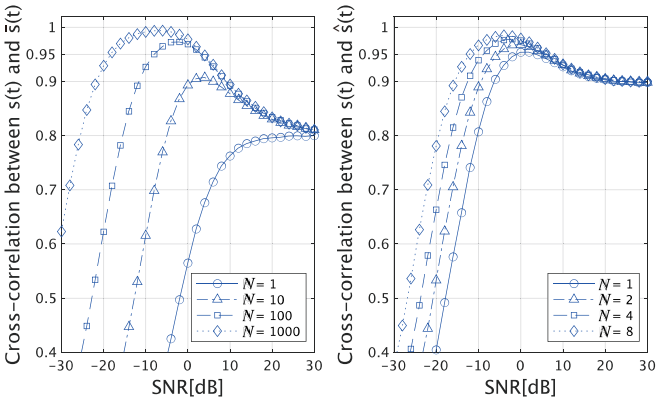

(a) Without LPF. (b) With LPF.

Fig. 2. Average cross-correlation between the source signal $s(t)$ and the reconstructed signals: (a) for $\bar{s}(t)$ (without LPF) and (b) for $\hat{s}(t)$ (with LPF).

B. Average Cross-Correlation Between Source and Lowpass-Filtered, Reconstructed Signals

To improve the smoothness of the reconstructed signal $\bar{s}(t)$, we employ a lowpass filter (LPF) as shown in Fig. 1. We assume that the LPF is linear and has an impulse response $h(t)$. In this paper, we employ an ideal LPF with a rectangular frequency response, which is realized using the DFT and yields a discrete-time lowpass-filtered, reconstructed signal $\hat{s}_i$ $(i = 1, 2, ..., M_s)$ such that $\hat{s}_i \leftrightarrow \hat{S}_k$ $(k = 1, 2, ..., M_s)$, where

$$\hat{S}_k = \begin{cases} \bar{S}_k \, (1 \le k \le M_B + 1, \; M_s - M_B + 1 \le k \le M_s) \\ 0 \quad (M_B + 2 \le k \le M_s - M_B) \end{cases}. \tag{2}$$

Here M_B is an integer that defines the bandwidth of the ideal LPF and $\bar{S}_k = \frac{1}{\sqrt{M_s}} \sum_{i=1}^{M_s} \bar{s}_i \, e^{-\mathrm{j}2\pi(i-1)(k-1)/M_s}$.

By defining a vector $\hat{\mathbf{s}} \in \mathbb{R}^{M_s \times 1}$, we can calculate the cross-correlation value between the source signal $s(t)$ and the lowpass-filtered, reconstructed signal $\hat{s}(t)$ such that $\mathbf{s}^{\mathcal{T}}\hat{\mathbf{s}}/(\sqrt{\mathbf{s}^{\mathcal{T}}\mathbf{s}}\sqrt{\hat{\mathbf{s}}^{\mathcal{T}}\hat{\mathbf{s}}})$. The cross-correlation values between $s(t)$ and $\hat{s}(t)$, which are averaged over 500 trials, vs SNR are shown in Fig. 2(b), where $M_B = 50$ was chosen for the pass bandwidth. Unlike in Fig. 2(a), N is chosen to be small such that N = 1, 2, 4, and 8 in Fig. 2(b), showing that with the LPF, the small N obtains significantly large cross-correlation values. Surprisingly, even for N = 1, the average cross-correlation value reaches 0.95 if SNR is appropriately chosen. This waveform reconstruction can be summarized as follows: For a certain normalization constant $\gamma \in \mathbb{R}$, $\gamma\hat{s}(t) \approx s(t)$ for $1 \le N \ll N'$ wrt the cross-correlation criterion if SNR is appropriate, where

$$\hat{s}(t) = h(t) * \left(\sum_{n=1}^{N} \mathrm{sgn}[s(t) + \xi_n(t)] \right). \tag{3}$$

Equation (3) is the basis for the design of highly efficient SRPAs for signals with large envelope fluctuations. In (3), the term $\mathrm{sgn}[s(t) + \xi_n(t)]$ takes binary values in $\{+1, -1\}$, which can be amplified using switching-mode (or saturation-mode) PAs (SMPAs) that achieve the maximum PA efficiency. Suppose that we use N SMPAs that have a common gain of K. In this case, the source signal $s(t)$ is efficiently amplified

and we obtain a K-fold amplified, reconstructed signal $K\hat{s}(t)$ such that

$$h(t) * \left(\sum_{n=1}^{N} K \cdot \mathrm{sgn}[s(t) + \xi_n(t)] \right) = K\hat{s}(t). \tag{4}$$

III. SR-Based PA Design for OFDM Signals

A. OFDM Signals

The complex envelope $z(t)$ of OFDM signals is given by

$$z(t) = \frac{1}{\sqrt{N_c}} \sum_{l=1}^{N_c} b_l \, e^{\mathrm{j}2\pi(l-1)t/T_0}, \ 0 \le t < T_0, \tag{5}$$

where N_c is the number of complex subcarriers, T_0 is the duration of OFDM signals, and $b_l = b_l^{(1)} + \mathrm{j}b_l^{(2)}$ is the complex message symbol that modulates the corresponding lth complex subcarrier $e^{\mathrm{j}2\pi(l-1)t/T_0}$ $(l = 1, 2, ..., N_c)$.

Without loss of generality, we assume 2PAM symbols for both $b_l^{(1)}$ and $b_l^{(2)}$, that is, $b_l^{(1)}, b_l^{(2)} \in \{+1, -1\}$. This corresponds to 4QAM or quaternary phase-shift keying (QPSK) for the lth complex subcarrier.

Using $z(t)$, the OFDM signals $f(t)$ are given by

$$f(t) = \Re\left[z(t)e^{\mathrm{j}2\pi f_c t}\right] \tag{6}$$

$$= x(t)\cos\omega_c t - y(t)\sin\omega_c t, \ \omega_c = 2\pi f_c, \tag{7}$$

where $x(t) = \Re[z(t)]$, $y(t) = \Im[z(t)]$, and f_c is the frequency for the first subcarrier ($l = 1$).

In the following, we assume that the discrete-time signals are sampled at time $t = (i-1)\Delta_t$ $(i = 1, 2, ..., N_c R_{\mathrm{os}})$, where $\Delta_t = T_0/(N_c R_{\mathrm{os}})$.

B. SR-Based PA Design

Using (4) and (7), we can readily obtain the structure of SRPAs as shown in Fig. 3, where $u_n(t)$ and $v_n(t)$ $(n = 1, 2, ..., N)$ are independent zero-mean Gaussian noises, which cause the SR effect, with a variance of $\mathrm{E}[u_n^2(t)] = \mathrm{E}[v_n^2(t)] = \sigma^2$. Since $\mathrm{E}[x^2(t)] = \mathrm{E}[y^2(t)] = 1$, $\mathrm{SNR} = \mathrm{E}[x^2(t)]/\mathrm{E}[u_n^2(t)] = \mathrm{E}[y^2(t)]/\mathrm{E}[v_n^2(t)] = 1/\sigma^2$ for all n. As for the discrete-time signals $u_{n,i}$ and $v_{n,i}$, $\mathrm{E}[u_{m,i}u_{n,j}] = \mathrm{E}[v_{m,i}v_{n,j}] = \delta_{m,n}\delta_{i,j}\sigma^2$ and $\mathrm{E}[u_{m,i}v_{n,j}] = 0$.

In Fig. 3, since all output signals $\bar{x}_n(t)$ and $\bar{y}_n(t)$ $(n = 1, 2, ..., N)$ from signum functions always take binary values in $\{+1, -1\}$, all input signals $\bar{x}_n(t)\cos\omega_c t - \bar{y}_n(t)\sin\omega_c t$ to the SMPAs have a constant envelope level of $\sqrt{\bar{x}_n^2(t) + \bar{y}_n^2(t)} = \sqrt{2}$. These signals are highly efficiently amplified through the SMPAs, and the subsequent bandpass filter (BPF) improves the quality of waveform reconstruction as in the LPF in Fig. 1. Thus, as the SMPA evolves, the PA efficiency of the SRPA improves.[2]

[2]For example, it is known that the maximum efficiency of a class-F amplifier increases with the number of harmonics, reaching 0.9045 when the number of harmonics is 5, and can theoretically approach 1 when the number of harmonics is increased [10].

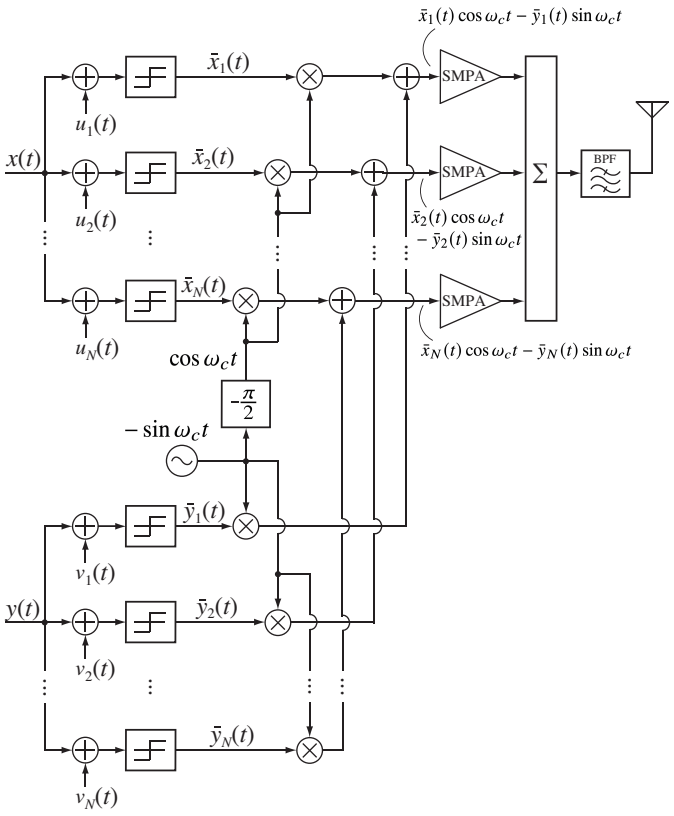

Fig. 3. Design of SR-based PAs.

C. Equivalent Lowpass Representation of SR-Based PAs

In order to simplify the analysis of communication systems, equivalent lowpass system representations are employed. Let $\eta_n(t)$ $(n = 1, 2, ..., N)$ be complex noises defined using $u_n(t)$ and $v_n(t)$ as $\eta_n(t) = u_n(t) + \mathrm{j}v_n(t)$. If we define a complex signum function $\mathrm{csgn}(z)$ as $\mathrm{csgn}(z) = \mathrm{sgn}(\Re[z]) + \mathrm{j}\,\mathrm{sgn}(\Im[z])$ $(z \in \mathbb{C})$, an equivalent lowpass system representation of the SRPAs is obtained as shown in Fig. 4, where Ks are intended as the gains of the SMPAs in Fig. 3 and the LPF is the equivalent lowpass system representation of the BPF in Fig. 3. This has an identical form to the summing network shown in Fig. 1 except for the difference in the real or complex system if $K = 1$. Therefore, $K\hat{z}(t)$ is obtained as the lowpass-filtered version of $K\bar{z}(t)$ as in Fig. 1, where $\bar{z}(t) = \sum_{n=1}^{N} \bar{z}_n(t)$ and $\bar{z}_n(t) = \mathrm{csgn}[z(t) + \eta_n(t)]$ as shown in Fig. 4.

In this paper, we employ an ideal BPF with a rectangular frequency response in Fig. 3. Therefore, the discrete-time signal $\hat{z}_i$ $(i = 1, 2, ..., N_c R_{\mathrm{os}})$ of $\hat{z}(t)$ is obtained such that

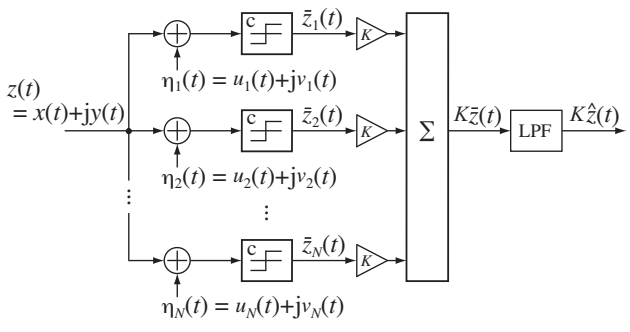

Fig. 4. Equivalent lowpass system representation of SR-based PAs.

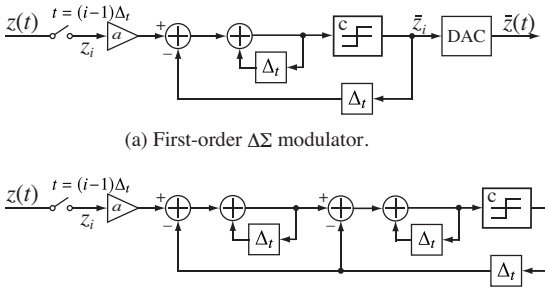

(a) First-order ΔΣ modulator.

(b) Second-order ΔΣ modulator.

Fig. 5. First- and second-order ΔΣ modulators models.

$\hat{z}_i \leftrightarrow \hat{Z}_k$ $(k = 1, 2, ..., N_c R_{\rm os})$, where

$$\hat{Z}_k = \begin{cases} \bar{Z}_k & (1 \le k \le N_c) \\ 0 & (N_c{+}1 \le k \le N_c R_{\rm os}) \end{cases} \tag{8}$$

and $\bar{Z}_k = \frac{1}{\sqrt{N_c R_{\rm os}}} \sum_{i=1}^{N_c R_{\rm os}} \bar{z}_i \, e^{-{\rm j}2\pi(i-1)(k-1)/(N_c R_{\rm os})}$.

Without loss of generality, we assume that $K = 1$ in the following discussions.

IV. Performance Evaluation

A. Coding Efficiency

As in Section II, the quality of waveform reconstruction in terms of cross-correlation values is improved by using the LPF; however, the energy contained in $\hat{z}(t)$ becomes smaller than that contained in $\bar{z}(t)$ owing to the LPF that discards the out-of-band spectral components contained in $\bar{z}(t)$. This energy loss caused by the LPF, equivalently, the energy loss caused by the BPF in Fig. 3, is called *coding efficiency CE* introduced by Johnson and Stapleton [20], which is given by CE = $\mathrm{E}[|\hat{z}(t)|^2]/\mathrm{E}[|\bar{z}(t)|^2] = \mathrm{E}[\hat{\mathbf{z}}^{\mathcal{H}}\hat{\mathbf{z}}]/\mathrm{E}[\bar{\mathbf{z}}^{\mathcal{H}}\bar{\mathbf{z}}]$.

B. ΔΣ Modulations

The CE has been used in the context of ΔΣ modulation-based PA (ΔΣPA) designs (see [20]–[23] and the references therein). In this paper, we consider a basic configuration of the first- and second-order ΔΣ modulators respectively shown in Figs. 5(a) and (b) for performance comparison, where each has an adjustable input gain a. The initial values stored in two memories in Fig. 5(a) and three memories in Fig. 5(b) for the time delay of Δ_t were all set to zero. Since the output signals $\bar{z}(t)$ (and also $\bar{z}_i$) from both ΔΣ modulators are obtained through the signum functions, their amplitudes become binary and are thus efficiently amplified by the SMPAs.

C. BER Characteristics

Figure 6 shows a transmission model that contains the output portion of the PA (transmitter) shown in Fig. 4 ($K = 1$) and the receiver including the OFDM demodulator in the presence of additive white Gaussian noise (AWGN) with two-sided power spectral density of $N_0/2$. Usually, the characteristics of BER are evaluated using the received energy per bit, E_b, defined using the received signal $\hat{z}(t)$. In this paper, the energy per bit, $\bar{E}_b$, defined using $\bar{z}(t)$ such that $\bar{E}_b = T_0\mathrm{E}[|\bar{z}(t)|^2]/(2N_c)$, is used. Consequently, the BER characteristics encompass both the impact of waveform distortion, as indicated by the cross-correlation, and the influence of energy loss, as quantified by the CE.

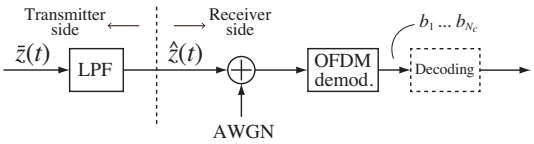

Fig. 6. Transmission model.

TABLE I
CEs for the uncoded and coded cases.

	ΔΣPAs		SRPAs			
	1st-order	2nd-order	$N=1$	$N=2$	$N=4$	$N=8$
Uncoded case	0.269	0.401	0.460	0.564	0.662	0.761
Coded case	0.451	0.717	0.736	0.740	0.786	0.837

In the following, N_c = 128, $R_{\rm os}$ = 32, and 4QAM (QPSK) message symbols for b_l are commonly considered. The design parameter SNR[3] for the SRPAs and the input gain a for the ΔΣPAs are set to minimize the required value of $\bar{E}_b/N_0$ that achieves BER $\approx 10^{-3}$.[4]

1) Uncoded Case: Figure 7(a) shows the BER characteristics of OFDM signals transmitted using SRPAs for N = 1, 2, 4, and 8 as a function of $\bar{E}_b/N_0$. Here, we assume that the uncoded message symbols are transmitted as b_l $(l = 1, 2, ..., N_c)$. An ideal curve, which is the case of $\hat{z}(t) = z(t)$ (distortionless transmission and no energy loss of CE = 1), is also plotted. The values of SNR and a were identified through simulations as given in Fig. 7(a), and the resultant CEs are summarized in Table I. It is verified from Fig. 7(a) that the BER performance improves as N increases, and the chosen SNR value becomes small as N increases. In other words, the required contribution of noises added for the SRPAs increases with N.

2) Coded Case: For practical system illustration, we use the standardized second-generation specification of the digital video broadcast standard (DVB-S2) [24] signal format, which uses low-density parity check (LDPC) coding.[5] The BER characteristics are shown in Fig. 7(b) for the coding rate of R_c = 1/3. CEs are summarized in Table I. It is observed from Fig. 7(b) that the SRPA of N = 1 and the second-order ΔΣPA have almost identical BER characteristics. It is seen that the SNR chosen for SRPA of N = 1 was SNR $\to \infty$, which means that the case without any noise (i.e., $\eta_1(t) = 0$) was the best. This is a valid conclusion only for N = 1 with powerful error correction such as R_c = 1/3.

The key advantage of using the SR approach over conventional ΔΣ-OFDM amplifying methods is clearly shown

[3]In a realistic scenario of analog circuit development, independent Gaussian noises can be introduced through amplifiers that generate thermal and shot noises with white power spectra, such as those observed over AWGN channels. The SNR value can be adjusted by attenuating the input signal power of the amplifier. The random variation of the comparator offset was employed as noise in [7].

[4]Thorough simulations were used to determine the optimal values of SNR and a.

[5]In addition, for the decoding, soft decisions are made using the approximated log-likelihood ratio, and the receiver has prior knowledge of signal power and channel noise variance. The maximum number of iterations was chosen to be 50. One packet for DVB-S2 consists of 64800 bits of a coded message, whereas one 4QAM-OFDM signal with $N_c = 128$ can carry only 256 bits. Therefore, the OFDM signals are transmitted 254 times repeatedly for the transmission of one packet, in which 224 dummy bits were included and were not used for decoding in our simulations.

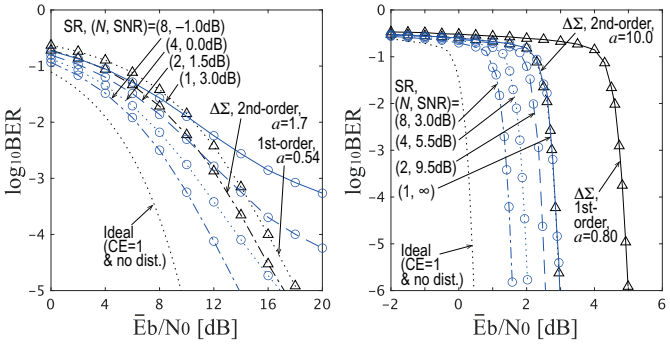

(a) Uncoded case. (b) Coded case ($R_c = 1/3$).

Fig. 7. BER characteristics of 4QAM(QPSK)-modulated OFDM signals transmitted using the SR- and $\Delta\Sigma$ modulation-based PAs ($N_c = 128$ and $R_{\rm os} = 32$).

in both parts of Fig. 7; (a) for the uncoded case and (b) for the coded case. In the uncoded case, our proposed design has an advantage over the conventional second-order methods of at least 1.6 dB for $N = 4$ improving to 3.1 dB for $N = 8$ at BER = 10^{-3}. For the coded case, with practical DVB-S2 signals, the advantage is more apparent for all values of N. This narrows the gap, relative to the ideal case[6], from 2.5 dB for the conventional second-order $\Delta\Sigma$PA to 1.1 dB for the new design SRPA of $N = 8$ at BER = 10^{-3}.

V. Conclusions

This paper has explored the use of the stochastic resonance concept for the transmission of OFDM signals. The cross-correlation studies of the N-path noise-aided summing network with lowpass filtering have shown that accurate signal reconstruction may be achieved for reasonable SNR values, even for small N. The concept has then been applied to a transmitter structure with power amplifiers and bandpass filtering. Detailed modelling of the signal transmission link in AWGN channel, with various values of N and appropriate SNR of the summing network, has shown advantages over $\Delta\Sigma$ modulation-based OFDM power amplification, in terms of BER performance improvement, even for the moderate value of $N = 8$, with only 1.1 dB energy consumption penalty relative to the ideal performance limit.[7] The results may open a new way of overcoming the power amplifier limitations of multicarrier systems, at the expense of a small energy consumption penalty and some increase in system complexity. Since all the optimal values of SNR depend on the target BER and N, system optimization will be required especially when fading channels are considered, and this is part of our ongoing work, as well as studies of appropriate predistortion techniques for higher order modulations, including optimal subcarrier power allocation.

References

[1] R. Benzi, A. Sutera, and A. Vulpiani, "The mechanism of stochastic resonance," *J. Phys. A: Math. Gen.*. vol. 14, L453–L457, 1981.

[2] R. Benzi, G. Parisi, A. Sutera, and A. Vulpiani, "Stochastic resonance in climatic change," *Tellus*, vol. 34, pp. 10–16, 1982.

[3] Y. Nakashima, T. Yamazato, S. Arai, H. Tanaka, and Y. Tadokoro, "Noise-aided demodulation with one-bit comparator for multilevel pulse-amplitude-modulated signals," *IEEE Wireless Commun. Lett.*, vol. 7, no. 5, pp. 848–851, Oct. 2018.

[4] A. Tatematsu, H. Hatano, K. Sanada, K. Mori, H. Tanaka, and Y. Tadokoro, "Noise-power estimation and performance improvement for SR-based receiver with few-bit ADC, " *NOLTA*, IEICE, vol. 14, no. 3, pp. 628–637, July 2023.

[5] J. J. Collins, C. C. Chow, and T. T. Imhoff, "Stochastic resonance without tuning," *Nature*, vol. 176, pp. 236–238, July 1994.

[6] J. L. Ceballos, I. Galton, and G.C. Temes, "Stochastic analog-to-digital conversion," *in Proc. 48th Midwest Symp. Circuits Syst.*, pp. 855–858 Aug. 2005.

[7] S. Weaver, B. Hershberg, P. Kurahashi, D. Knierim, and U.-K. Moon, "Stochastic flash analog-to-digital conversion," *IEEE Trans. Circuits Syst. I, Reg. Papers*, vol. 57, no. 11, pp. 2825–2833, Nov. 2010.

[8] A. Tsukahara, S.-G. Cho, K. Tanaka, A. Homma, Y. Uchikawa, "Design and trial production FPGA based stochastic resonance circuit using LVDS and an examination for surface EMG measurement," *in Proc. 62nd SICE Annual Conference*, pp. 345–350, Sept. 2023.

[9] A. Goda, C. Matsui, and K. Takeuchi, "Stochastic resonance modeling of floating gate-based neurons in summing networks for accurate and energy-efficient operations, " *IEEE Trans. Electron Devices*, vol. 71, no. 3, pp. 1737–1744, March 2024.

[10] F. H. Raab, P. Asbeck, S. Cripps, P. B. Kenington, Z. B. Popović, N. Pothecary, J. F. Sevic, and N. O. Sokal, "Power amplifiers and transmitters for RF and microwave," *IEEE Trans. Microw. Theory Techn.*, vol. 50, no. 3, pp. 814–826, March 2002.

[11] H. Ochiai, "An analysis of band-limited communication systems from amplifier efficiency and distortion perspective," *IEEE Trans. Commun.*, vol. 61, no. 4, pp. 1460–1472, April 2013.

[12] B. Razavi, "75 years of RF design: Highlights and paradigm shifts," *IEEE Solid-State Circuits Mag.*, vol. 15, no. 3, pp. 62–79, Aug. 2023.

[13] G. Nikandish, R. B. Staszewski, and A. Zhu, "Breaking the bandwidth limit: A review of broadband Doherty power amplifier design for 5G, " *IEEE Microw. Mag.*, vol. 21, no. 4, pp. 57–75, April 2020.

[14] X. Zhang, S. Li, D. Huang, and T. Chi, "A millimeter-wave three-way Doherty power amplifier for 5G NR OFDM," *IEEE J. Solid-State Circuits*," vol. 58, no. 5, pp. 1256–1270, May 2023.

[15] M. Litchfield and T. Cappello, "The various angles of outphasing PAs: Competitiveness of outphasing in efficient linear PA applications," *IEEE Microw. Mag.*, vol. 20, no. 4, pp. 135–145, April 2019.

[16] S. Kimura and T. Kawasaki, "How to design an outphasing power amplifier with digital predistortion," *IEICE Trans. Electron.*, vol. E104-C, no. 10, pp. 472–479, Oct. 2021.

[17] C. Hu, W Shi, R. Yang, S. Lin, Z. Dai, R. Gao, C. Huang, J. Pang, and M. Li, "Design of an outphasing power amplifier using complex combining method for broadband application," *IEEE Microw. and Wireless Techn. Lett.*, vol. 33, no. 4, pp. 443–446, April 2023.

[18] C.-H. Kuo, J.-T.Yeh, J.-H. Chen, and Y.-J. E. Chen, "A dual-phase center-aligned 7-bit digital pulsewidth modulator for polar transmitters," *IEEE Trans. Microw. Theory Techn.*, vol. 70, no. 11, pp. 5205–5212, 2022.

[19] P. Zhou, X. Ruan, N. Liu, and Y. Wang, "A series-parallel-form switch-linear hybrid envelope tracking power supply with two multilevel converters sharing a voltage-level provider," *IEEE Trans. Power Electron.*, vol. 38, no. 1, pp. 593–603, Jan. 2023.

[20] T. Johnson and S. P. Stapleton, "RF class-D amplification with bandpass sigma-delta modulator drive signal," *IEEE Trans. Circuits Syst. I, Reg. Papers*, vol. 53, no. 12, pp. 2507–2520, Dec. 2006.

[21] M. M. Ebrahimi, M. Helaoui, and F. M. Ghannouch, "Delta-sigma-based transmitters: Advantages and disadvantages," *IEEE Microwave Mag.*, vol. 14, no. 1, pp. 68–78, Jan.–Feb. 2013.

[22] M. Jouzdani, M. M. Ebrahimi, M. Helaoui, and F. M. Ghannouchi, "Complex delta-sigma-based transmitter with enhanced linearity performance using pulsed load modulation power amplifier," *IEEE Trans. Microw. Theory Techn.*, vol. 65, no. 9, pp. 3324–3335, Sept. 2017.

[23] N. Kumar and K. Rawat, "Coding efficiency enhancement using time-interleaved level splitting and optimized multi-level delta sigma modulation in digital transitter," *IEEE Trans. Circuits Syst. I, Reg. Papers*, vol. 68, no. 7, pp. 2986–2997, July 2021.

[24] ETSI Standard EN 302 307 V1.4.1: Digital Video Broadcasting (DVB); Second generation framing structure, channel coding and modulation systems for broadcasting, interactive services, news gathering and other broadband satellite applications (DVB-S2), European Telecommunications Standards Institute, 2005-03.

[6] In this paper, the ideal case is defined as distortionless transmission and CE = 1. This gives the optimal results in the context of our discussion, achieving quasi error free, defined as a packet error rate of 10^{-7}, at $\bar{E}_b/N_0 = 0.59$ dB for R_c = 1/3 [24].

[7] As for the coded 16QAM with Gray encoding, the energy consumption penalty was approximately 1.3 dB for $N = 8$, while for the uncoded 16QAM, $N \geq 10$ was required to attain BER $\approx 10^{-3}$; it was obtained at $\bar{E}_b/N_0$ = 26.0 dB and 17.1 dB for $N = 10$ and 16, respectively.